Edge Localized Mode Control in DIII-D Using Magnetic Perturbation-Induced Pedestal Transport Changes

R.A. Moyer 1), K.H. Burrell 2), T.E. Evans 2), M.E. Fenstermacher 3), P. Gohil 2), I. Joseph 1), T.H. Osborne 2), M.J. Schaffer 2), P.B. Snyder 2), J.G. Watkins 4), L.R. Baylor 5), M. Bécoulet 6), J.A. Boedo 1), N.H. Brooks 2), E.J. Doyle 7), K.-H. Finken 8), P. Garbet 6), M. Groth 3), J. Harris 5) E.M. Hollmann 1), G.L. Jackson 2), M. Jakubowski 8), T.C. Jernigan 5), S. Kasilov 9), C.J. Lasnier 3), A.W. Leonard 2), M. Lehnen 8), J. Lönnroth 10), E. Nardon 6), V. Parail 11), G.D. Porter 3), T.L. Rhodes 7), D.L. Rudakov 1), A. Runov 12), O. Schmitz 8), R. Schneider 12), D.M. Thomas 2), P. Thomas 6), G. Wang 7), W.P. West 2), L. Yan 13), J.H. Yu 1), and L. Zeng 7)

1) University of California-San Diego, La Jolla, California, USA
2) General Atomics, San Diego, California, USA
3) Lawrence Livermore National Laboratory, Livermore, California, USA
4) Sandia National Laboratories, Albuquerque, New Mexico, USA
5) Oak Ridge National Laboratory, Oak Ridge, Tennessee, USA
6) Association EURATOM-CEA, Cadarache, France
7) University of California-Los Angeles, Los Angeles, California, USA
8) Forschungszentrum Julich, Association EURATOM-FZJ, Trilateral Euregio Cluster, Germany
9) Kharkov Institute for Physics and Technology, Kharkov, Ukraine
10) Association EURATOM-Tekes, Helsinki University of Technology, Finland
11) EURATOM/UKAEA Fusion Association, Culham Science Center, United Kingdom
12) Max Planck Institute, Greifswald, Germany
13) Southwest Institute for Physics, Chengdu, China

email: moyer@fusion.gat.com

Abstract. Edge resonant magnetic perturbations (RMPs) with toroidal mode numbers $n = 3$ have been used in DIII-D to eliminate Type I edge localized modes (ELMs) when the edge safety factor is in the resonant window $3.4 < q_{95} < 3.7$ without degrading confinement in H-modes with ITER-relevant pedestal collisionalities $\nu_e^* \sim 0.2$. The RMP reduces ∇p_{ped} as expected, with ∇p_{ped} controlled by the RMP amplitude. Linear peeling-ballooning (P-B) stability analysis indicates that the ELMs are suppressed by reducing ∇p_{ped} below the P-B stability limit. The ∇p_{ped} reduction results primarily from changes in the pedestal density n_e profile, not the pedestal electron temperature T_e profile. This result is inconsistent with estimates based on quasi-linear stochastic diffusion theory using the vacuum field (no screening of the RMP). The particle transport increase is accompanied by changes in toroidal rotation, radial electric field, and density fluctuation level $\tilde{n}$ in the pedestal, suggesting increased fluctuation-driven particle transport.

1. Introduction

Operation of next-step burning plasma devices with high fusion power gain Q_{fus} requires operation at high pedestal pressures that lead to repetitive MHD instabilities known as edge localized modes (ELMs). In ITER, for example, achieving the target $Q_{\text{fus}} = 10$ is predicted to produce Type I ELMs with energy losses that exceed the ablation temperature of graphite [1] and limit the divertor lifetime [2]. Consequently, a technique that replaces the impulsive ELM-induced transport with more continuous transport while preserving the H-mode pedestal height and core performance would significantly improve the viability of ITER. Several approaches to controlling the impulsive power loading due to ELMs are being studied, including: ELM-free H-modes (QH mode [3]), small ELM regimes [4], and H-modes with pellet-triggered ELMs [5]. Another approach is to use edge resonant magnetic perturbations (RMPs) to enhance transport in the pedestal enough to reduce the pedestal pressure gradient

∇p_{ped} below the stability limit for Type I ELMs. In DIII-D, RMPs with toroidal mode number $n = 3$ were used to eliminate Type I ELMs when the edge safety factor is in the resonant window $3.4 < q_{95} \sim 3.7$ without significantly degrading confinement in H-modes with ITER-relevant pedestal collisionalities $\nu_e^* \sim 0.2$ in both low [6-8] and high triangularity shapes.

In this paper, we present the results of ELM suppression experiments using an edge RMP in H-modes with ITER-relevant ν_e*. It is found that the RMP reduces ∇p_{ped} [6], with the ∇p_{ped} decrease controlled by the RMP amplitude. Linear peeling-ballooning (P-B) stability calculations using the ELITE code [9] indicate that the ∇p_{ped} reduction stabilizes the P-B modes associated with Type I ELMs [6-8]. The ∇p_{ped} reduction is primarily due to reduction of the pedestal density n_e, not the pedestal electron temperature T_e [7,8]. This result is inconsistent with expectations from quasi-linear theory using the applied RMP (no screening) [7] and with simulations of the thermal transport in the stochastic layer using the fluid Monte Carlo heat transport code E3D with the applied RMP [10]. ELM suppression is accompanied by an increase in density fluctuations $\tilde{n}$ due to core modes and broadband turbulence in the pedestal, suggesting that particle transport increases due to turbulent transport.

2. RMP Approach to ELM Suppression

In the original RMP ELM suppression concept [11], an edge RMP $\delta b_r^{m,n}$ produces islands on rational surfaces in the pedestal. For large enough $\delta b_r^{m,n}$ inside the plasma, these islands overlap, producing a stochastic layer. The enhanced radial transport reduces the edge p_{ped} and ∇p_{ped} [Fig. 1(a)], moving the pedestal into the stable portion of the P-B stability diagram [Fig. 1(b)]. Several features of H-mode pedestals in poloidally diverted tokamaks should facilitate RMP ELM suppression by localizing the perturbation to the pedestal: 1) the high magnetic shear which leads to closely spaced rational surfaces in the pedestal, so that less $\delta b_r^{m,n}$ is needed to generate the stochastic layer [11]; 2) the plasma rotation gradient across the pedestal, weakening rotational screening of the RMP [12,13]; 3) the plasma pressure gradient across the pedestal, weakening the pressure screening of the RMP [14]; and 4) the plasma collisionality increase across the pedestal, reducing the RMP screening and enhancing the transport [15].

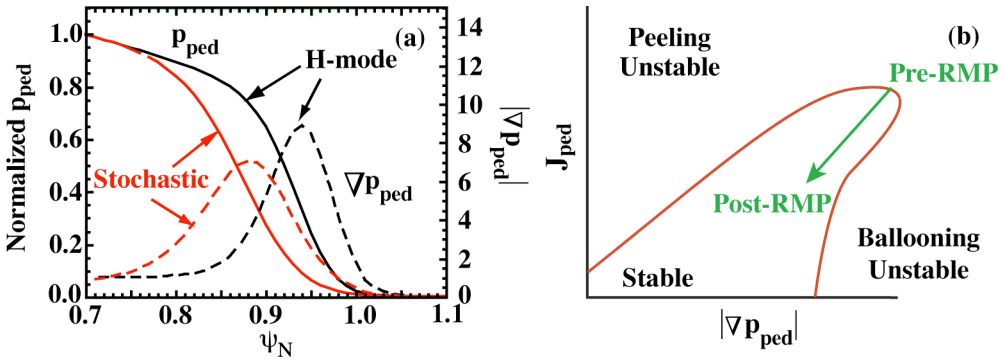

FIG. 1. (a) Schematic of ELMing H-mode (black) and RMP-assisted ELM-free H-mode (red) profiles of pedestal pressure p_{ped} (solid) and pressure gradient ∇p_{ped} (dashed). (b) Schematic of the P-B stability diagram (J_{ped}, $|\nabla p_{ped}|$) showing how the ∇p_{ped} drop moves the pedestal diagonally (green arrow) from the unstable to the stable region due to dependence of the bootstrap current on ∇p_{ped}.

In DIII-D, the RMP is provided by a flexible set of coils inside the vacuum vessel (the "I-coil"), consisting of 2 sets of 6 single-turn window-frame coils, mounted above and below

the outboard midplane. For these experiments, the I-coil was operated with a toroidal mode number $n = 3$ and strong edge resonant poloidal harmonics $6 < m < 13$ [Fig. 2(a)] that produce weakly overlapping vacuum field islands and a broad stochastic layer with remnant islands in the absence of screening by rotation or pressure [Fig. 2(b)].

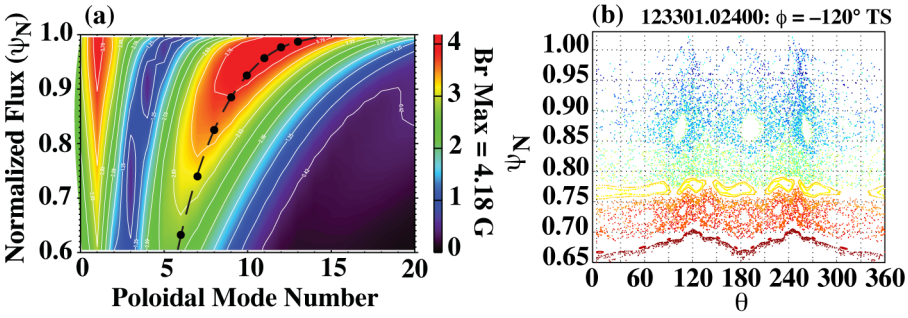

FIG. 2. (a) Color contour plot of the magnetic perturbation spectrum, showing the Fourier amplitude of the $n = 3$ vacuum field from a 2 kA I-coil current in discharge 122344 as a function of poloidal mode number m and normalized poloidal flux ψ_n. Contributions from measured field errors are included. White contour lines are drawn at each 10% in amplitude. Mode resonances $m = nq(\psi_n)$ (•) lie along a ridge in the contours of the perturbing field. The color bar shows the amplitude scale in Gauss. (b) Poincaré plot of the vacuum perturbed magnetic field in the (θ,ψ_n) plane for $\phi = -120°$ in discharge 123301 at 2400 ms.

Pedestal collisionality ν_e^* is an important parameter in these experiments because the fraction $\Delta W_{ELM}/W_{PED}$ of the pedestal stored energy W_{PED} lost in an ELM (ΔW_{ELM}) increases as ν_e^* decreases, reaching 20% at ITER-relevant ν_e^* [1]. In addition, ν_e^* is predicted to impact both the penetration of the perturbation $\delta b_r^{m,n}$ [15] and the stochastic layer transport rates. Consequently, performing the RMP ELM control experiments at ITER-relevent pedestal ν_e^* is important. In DIII-D, ITER-like values of pedestal ν_e^* based on generalization of the Sauter formula [16] for $Z_{eff} > 1$ [17] are achieved by pumping the DIII-D divertor. In the initial $\nu_e^* \sim 0.2$ RMP ELM suppression experiments, divertor pumping required operation at much lower triangularity $\delta = 0.37$ than that planned for ITER [Fig. 3(a)]. With installation of a new divertor baffle structure in 2005, divertor pumping became possible with $\delta \sim 0.7$ in ITER similar shapes (ISS) [Fig. 3(b)].

3. Characterization of the ELM-Suppressed State

Large ELMs have been completely eliminated in ELMing H-modes with $\nu_e^* \sim 0.2$ for both $\delta \sim 0.37$ (black) and $\delta \sim 0.7$ (red), as shown in Fig. 3(c). In each shape, the ELMing H-mode is replaced by a quiescent, steady-state RMP-assisted ELM-free H-mode with confinement quality factor $H_{98y2} \approx 1$. For $\delta \sim 0.7$, the discharge is switched from 100% co-plasma current neutral beam injection (co-NBI) to 18% counter-NBI at 4000 ms, producing a drop in pedestal toroidal rotation v_ϕ followed by a return to ELMing H-mode at 4105 ms. For each δ, the pedestal v_ϕ increases when the ELMs cease. This pedestal spin-up is a feature of ELM suppression discharges that lack core MHD and maintain high performance, particularly at high δ. The I-coil current needed to suppress ELMs increases at high δ, in part because the rational surfaces are further from the I-coils (Fig. 3). The I-coil currents of 3 kA ($\delta \sim 0.37$) and 4 kA ($\delta \sim 0.7$) in Fig. 3 correspond to an increase in the $\delta b_r^{11,3}$ Fourier amplitude normalized to the toroidal magnetic field B_T from $\delta b_r^{11,3}/B_T = 2.8\text{x}10^{-4}$ to $3.4\text{x}10^{-4}$ and are representative of the increased current needed to stabilize ELMs at high δ.

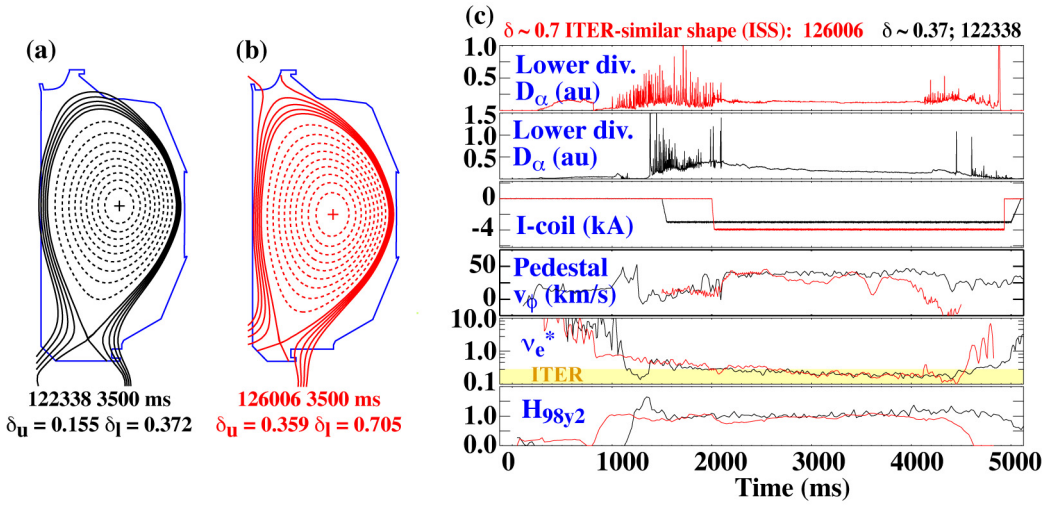

FIG. 3. Plasma shapes for the RMP ELM suppression experiments at $\nu_e^* \sim 0.2$ with (a) $\delta \sim 0.37$ and (b) $\delta \sim 0.7$ in an ITER-similar shape (ISS). (c) ELM suppression at $\nu_e^* \sim 0.2$ for the $\delta \sim 0.37$ (black) and $\delta \sim 0.7$ (red) shapes, showing, top to bottom: lower divertor recycling, I-coil current, pedestal toroidal rotation v_ϕ, ν_e^*, and H-mode confinement quality factor H_{98y2}.

Application of 2 kA of I-coil current significantly reduces ∇p_{ped} as shown in Fig. 4(a). This reduction in the peak and width of ∇p_{ped}^{TOT} is accompanied by a shift in the radius of the peak, which is also important for P-B stability. Increasing the I-coil current to 3 kA narrows ∇p_{ped}^{TOT} further, and shifts the radius of the peak gradient further out. The ∇p_{ped}^{TOT} is roughly twice ∇p_{ped}^{e}, indicating that the electron and ion channels share nearly equally in the ∇p_{ped} reduction [Fig. 4(a,b)]. The ∇p_{ped} modifications in Fig. 4(a) result primarily from changes in the pedestal n_e profile, not the T_e profile, as shown in Fig. 4(c). This n_e drop results from a substantial density pump-out when the RMP is applied, as has been reported in previous stochastic boundary experiments [18,19]. As the density pumps out, the ion and electron channels decouple, leading to an increase in T_i in the core to as high as 20 keV. This increase in T_i/T_e alters the partition of energy between the ions and electrons, increasing the power in the electron channel through the pedestal.

4. Peeling-Ballooning Stability Analysis of RMP-Assisted ELM-Free H-Modes

In experiments at $\nu_e^* \sim 0.2$, it is found that, within experimental uncertainties, the RMP ELM-free discharges are stable to P-B modes, whereas ELMing discharges become unstable to P-B modes just before an ELM occurs [6-8]. Profile data similar to that shown in Fig. 4 are used in a 2D stability code (ELITE [9]) to evaluate the P-B stability for an extensive set of ELMing and RMP-assisted ELM-free discharges. The stability calculations are based on accurate global reconstructions of full plasma profiles along with a broad range of mode numbers (n = 5–30). The non-local stability results are represented in a simplified manner in Fig. 5. Here, the global experimental profiles are characterized by representative local values, and the results displayed in a single stability diagram to facilitate comparisons. The variation in plasma conditions for the discharges in Fig. 5 modifies the stability threshold for γ_N but it remains between 0.5 and 2 for all the discharges shown, and we have chosen a nominal instability threshold boundary of $\gamma_N = 1$ to represent this band in the figure. Figure 5 shows that in RMP-assisted ELM-free discharges (ellipses) the normalized growth rate lies inside the stable region when the error bars on the data are taken into consideration. On the other hand, ELMing discharges (diamonds) consistently reside outside the stability boundary.

Figure 5 also shows that by increasing the I-coil current, the RMP-assisted ELM-free discharges can be made deeply stable (red I-coil current labels).

5. RMP-Induced Pedestal Transport Changes

Pellet perturbation experiments have been used to investigate the particle balance changes due to the I-coil (Fig. 6). Identical pellets were injected into three $\delta \sim 0.7$ discharges with similar recycling: (blue) ELMing H-mode (I-coil = 0 kA; 100% co-NBI), (red) RMP-assisted ELM-free H-mode (I-coil = 4 kA; 100% co-NBI), and (black) RMP-assisted ELM-free H-mode (I-coil = 4 kA; 20% counter-NBI). The density perturbation Δn_e decayed twice as fast in the RMP-assisted ELM-free H-modes as in the ELMing H-mode, suggesting that part of the change in mean ion residence time τ_p* is due to increased particle transport.

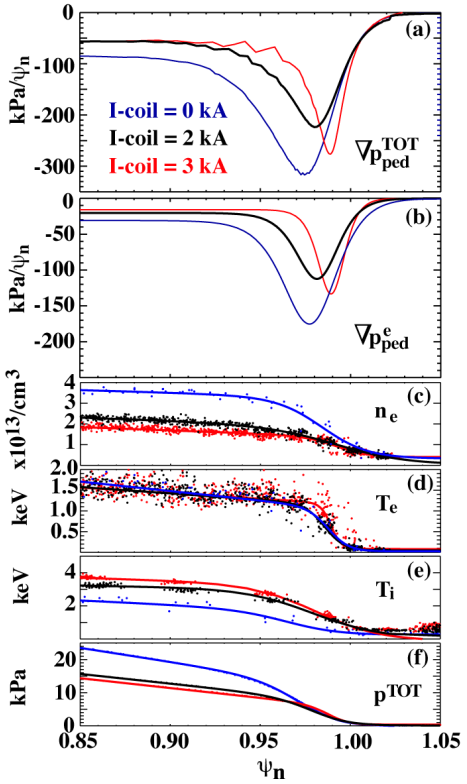

FIG. 4. (a) Pedestal total pressure gradient and (b) electron pressure gradient versus I-coil current in $\delta \sim 0.37$ discharges. (c) Pedestal profiles of (top to bottom) n_e, T_e, T_i, and p^{TOT} vs I-coil current. Dots are data points; lines are hyperbolic tangent fits to the data. The profile for 0 kA (blue) is obtained by fitting Thomson and CER data in the last 20% of the ELM cycle. The 2 kA (yellow) and 3 kA (red) profiles are fits to all Thomson and CER data in 500 ms windows during ELM suppression.

The small T_e profile changes are unexpected from quasi-linear theory [8,19,20]. For $0.85 < \psi_n <$

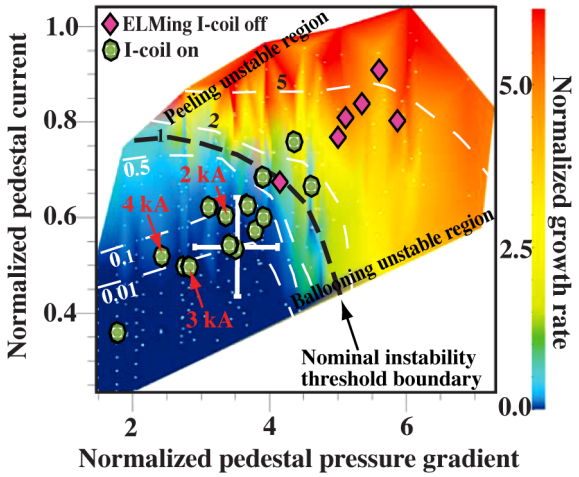

FIG. 5. Normalized P-B mode growth rates $\gamma_N = \gamma/(0.5\omega_{*e})$ (where γ is the P-B growth rate and ω_{*e} is the electron diamagnetic drift frequency) for 6 ELMing cases (diamonds) just before an ELM and 14 RMP-induced ELM-free (ellipses) cases. γ_N is plotted as a function of the maximum value of the normalized pedestal pressure gradient $\alpha = -[\mu_o/(2\pi)^2]\partial V/\partial\psi(V/2\pi^2 R_o)(\partial p/\partial\psi)$ (where V is the plasma volume, p is the pressure, ψ is the poloidal magnetic flux and R_o is the major radius of the plasma) and a characteristic pedestal current density j_N^{ped}, which is taken to be the peak value of the parallel current in the pedestal normalized by the average parallel current in the pedestal. The stability boundary (black dashed line). Representative error bars, denoting one standard deviation, are shown on the data point at $\alpha = 3.4$ and $j_N^{ped} = 0.53$. The color bar shows the value of γ_N for the color contours in the plot.

0.98, the T_e profile flattens and 1D power balance estimates indicate that $\chi_e^{exp} = -q_e/n_e \nabla T_e$, where q_e is the heat flux in the electron channel, increases to 2.8 m^2s^{-1} for the 3 kA case in Fig. 4. For $0.985 < \psi_n < 1$, the T_e profile *steepens* and the 1D power balance estimate is $\chi_e^{exp} = 0.1$ m^2s^{-1}. Comparing these experimental estimates with the quasi-linear estimate of $\chi_{m,n}^{ql} = v_{Te} D_{m,n}^{ql} = 49$ m^2s^{-1}, where v_{Te} is the electron thermal speed and $D_{m,n}^{ql} = \pi R_o \sum_{m=11-13}^{n=3} q_{m,n} (\delta b_r^{m,n} B_T^{-1})^2(m) = 3.5\times10^{-6} m$ is the magnetic field diffusivity [7,8], yields $\chi_{m,n}^{ql} / \chi_e^{exp} \sim 18$ at the top of the pedestal, which is a modest difference given the uncertainties in the estimate. In the steep gradient region ($\psi_n > 0.985$), $\chi_{m,n}^{ql} / \chi_e^{exp} \sim 500$. This result is difficult to explain with quasi-linear theory, especially because in this region, screening of the RMP is predicted to be small [15].

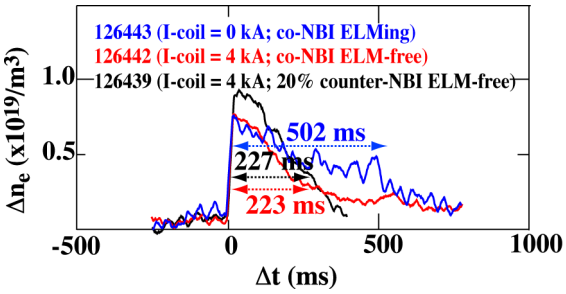

FIG. 6. Decay of pellet-induced density rises Δn_e in: (blue) ELMing H-mode with I-coil = 0 kA, (red) RMP-assisted ELM-free H-mode with 100% co-NBI, and (black) RMP-assisted ELM-free H-mode with 20% counter-NBI. The discharges have similar divertor recycling behavior.

Applicability of quasi-linear theory to these discharges is limited by the relatively weak stochasticity and the presence of multiple remnant islands [Fig. 2(b)]. To address this limitation, the magnetic field model from the TRIP3D code [11] has been used in the fluid heat transport code E3D [10,21] to simulate heat transport in the weakly stochastic magnetic field. Preliminary results, neglecting self-consistent density evolution and atomic physics, indicate that the electron heat transport estimated using the vacuum field exceeds that measured in the experiment by a significant amount [10]. This discrepancy may arise from use of the full vacuum RMP without inclusion of shielding by plasma rotation or breakdown of the fluid model in this $\nu_e^* \sim 0.2$ regime. [10].

Comparison of the small changes in the T_e profile measured during the RMP [Fig. 4(c)] with expectations for stochastic layer transport is complicated by some effects which need to be better understood. The large T_i rise in the core during the RMP should increase the power in the electron channel q_e at the top of the pedestal at the same time that n_e drops by a third, increasing the power/particle. These effects might limit the decrease in pedestal T_e expected for a stochastic layer except near the separatrix where the collisional coupling re-equilibrates the ion/electron power split.

6. Evidence for Penetration of the RMP

The discrepancy between theoretical and experimental power balance estimates of the electron thermal transport emphasizes the need to understand $\delta b_r^{m,n}$ inside the plasma. Several measurements indicate that the RMP penetrates at least the last few percent of ψ_n, including the existence of a narrow resonance in q-value $3.4 < q_{95} < 3.7$ for the ELM suppression. Langmuir probe measurements near the divertor strike point also show an increase in T_e and a large drop in floating potential to -150 V, indicating the presence of hot electrons in the divertor during the RMP [22]. These measurements are consistent with the connection of magnetic field lines from within the H-mode pedestal to the divertor target plates, leading to a flux of hot electrons (not thermalized in the SOL) to the targets. The radial electric field on the SOL side of the E_r well becomes strongly positive, consistent with formation of a

stochastic layer, while the persistence of the $E_r < 0$ minimum in the H-mode E_r well may indicate that the RMP doesn't fully penetrate past this point in the pedestal [Fig. 7(b)].

Further evidence for RMP penetration comes from comparison of the measured splitting of the divertor strike point with predictions of the intersection of homoclinic tangles with the target plates. The RMP splits the separatrix into stable and unstable manifolds which oscillate with increasing amplitude near the divertor X-point, forming "homoclinic tangles" [23]. These manifolds have been calculated using TRIP3D, and have been shown to govern the T_e profile with E3D [10]. The predicted T_e structures are seen in carbon line emission from the X-point region during RMP-assisted ELM-free H-modes [10,24]. The intersection of the tangles with the divertor target plates produces a spiral pattern on the target plates that has been calculated with TRIP3D and compared to measurements in RMP-assisted ELM-free H-modes at $\nu_e^* \sim 1$ [25]. The observed splitting at $\nu_e^* \sim 1$ exceeds the predicted splitting by 3, implying *amplification* of the vacuum $\delta b_r^{m,n}$. Preliminary comparisons of the predicted and observed splitting in RMP-assisted ELM-free H-modes at $\nu_e^* \sim 0.2$ [24,25] suggest that there is less amplification near the separatrix at this collisionality, consistent with expectations from an analytical screening model [13].

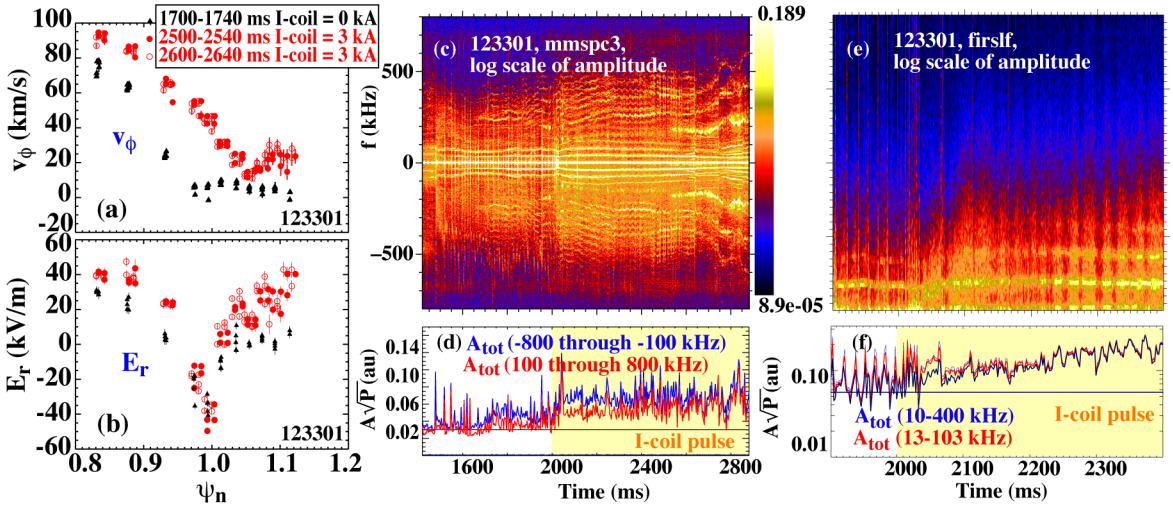

FIG. 7. Pedestal (a) v_ϕ and (b) E_r profiles during the ELMing phase before the I-coil and at two times during the RMP-assisted ELM-free H-mode for discharge 123301 with $\nu_e^* \sim 0.2$ and $\delta \sim 0.37$. (c) $\tilde{n}$ amplitude spectrum and (d) rms amplitudes A_{tot} for frequencies (blue) <0 kHz and (red) >0 kHz versus time for $k_\theta = 1\pm1$ cm^{-1} (FIR scattering). (e) $\tilde{n}$ amplitude spectrum and (f) rms amplitudes for (blue) 10-400 kHz and (red) 13-100 kHz for a channel reflecting at $n_e = 1.3\times10^{13}$ cm^{-3} ($\psi_n = 0.98$) in the pedestal.

7. Mechanisms for Increased Pedestal Particle Transport

ELM suppression in $\nu_e^* \sim 0.2$ discharges is accompanied by changes to v_ϕ, E_r and density fluctuations $\tilde{n}$ in the core and pedestal. The v_ϕ increase occurs across the pedestal and SOL on a 50 ms timescale [Fig. 7(a)], but is largest near the separatrix where $v_\phi \approx 0$ in $\nu_e^* \sim 0.2$ discharges at $\delta \sim 0.37$. This minimum in v_ϕ becomes a well (counter-I_p rotation, $v_\phi < 0$) at higher $\delta \sim 0.7$. On the same timescale as the pedestal v_ϕ increase, the H-mode E_r well narrows as E_r increases both inboard and outboard of the E_r minimum [Fig. 7(b)]. This change increases E_r shear outside of $\psi_n \approx 0.9$, but reduces E_r shear for $\psi_n < 0.9$. There is an increase in $\tilde{n}$ for poloidal wavenumbers $k_\theta = 1\pm1$ cm^{-1} during ELM suppression [Fig. 7(d)] as measured by FIR coherent scattering. This increase results from increases in both coherent mode activity as well as increases in the broadband ñ level as seen in Fig. 7(c)] (these changes are not spatially

localized by this measurement). Radially localized measurements from homodyne reflectometry in the pedestal also show changes in the character of the fluctuations [Fig. 7(e)] and in the overall amplitude [Fig. 7(f)]. These $\tilde{n}$ changes suggest that the changes in particle balance may result from increased particle convection due to either ion scale drift wave turbulence or convective cells.

8. Conclusions

An $n = 3$ edge RMP has been used in DIII-D to eliminate Type I ELMs when the edge safety factor is in the resonant window $3.4 < q_{95} < 3.7$ without significantly degrading confinement in H-modes with ITER-relevant pedestal collisionality $\nu_e^* \sim 0.2$. The results indicate that the applied RMP penetrates at least far enough into the pedestal to reduce ∇p_{ped} below the P-B stability limit for Type I ELMs by altering the global particle balance (the particle confinement time and/or recycling). The effect on heat transport is significantly less than expected from quasi-linear theory using the applied RMP (no screening) or from simulations of the heat transport in a stochastic layer using the fluid Monte Carlo heat transport code E3D with the full applied RMP. The increase in density fluctuations in the pedestal suggests that particle transport rises due to increased turbulent transport. Recent extension of RMP-assisted ELM-free H-mode operation to $\delta \sim 0.7$ ITER-similar shapes at low ν_e^* indicates that RMP ELM suppression is a promising tool for ITER.

Work supported in part by the U.S. Department of Energy under DE-FG02-04ER54758, DE-FC02-04ER54698, DE-FG02-05ER54809, W-7405-ENG-48, DE-AC04-94AL85000, DE-AC05-00OR22725, and DE-FG03-01ER54615.

References

[1] LOARTE, A., *et al.*, Plasma Phys. Control. Fusion **45** (2003) 1549.
[2] FEDERICI, G., *et al.*, J. Nucl. Mater. **313-316** (2003) 11.
[3] BURRELL, K.H., *et al.*, Phys. Plasmas **12** (2005) 056121.
[4] SAARELMA, S., GUNTER, G., and HORTON, L.D., Nucl. Fusion **43** (2003) 262.
[5] LANG, P.T., *et al.*, Nucl. Fusion **44** (2003) 665.
[6] BURRELL, K.H., *et al.*, Plasma Phys. Control. Fusion **47** (2005) B37.
[7] EVANS, T.E., *et al.*, Nature Physics **2** (2006) 419-423
[8] EVANS, T.E., *et al.*, Phys. Plasmas **13** 056121 (2006).
[9] WILSON, H.R., *et al.*, Phys. Plasmas **9** (2002) 1277. P.B. Snyder, *et al.*, Phys. Plasmas **9** 2037 (2002).
[10] JOSEPH, I., *et al.*, J. Nucl. Mater. in press (2006).
[11] EVANS, T.E., MOYER, R.A., and MONAT, P., Phys. Plasmas **9** (2002) 4957.
[12] FITZPATRICK, R., Phys. Plasmas **5** (1998) 3325.
[13] PARAIL, V., *et al.*, this conference.
[14] BOOZER, A.H., Phys. Plasmas **10** (2003) 1458.
[15] BECOULET, M., *et al.*, this conference.
[16] SAUTER, O., ANGIONI, C., and LIN-LIU, Y.R., Phys. Plasmas **6** (1999) 2834.
[17] WEST, W.P., and BURRELL, K.H., Private communication (2006).
[18] McCOOL, S.C., *et al.*, Nucl. Fusion **30** (1990) 167.
[19] GHENDRIH, Ph., GROSMAN, A., and CAPS, H., Plasma Phys. Control. Fusion **38** (1996) 1653.
[20] RECHESTER, A.B., and ROSENBLUTH, M.N., Phys. Rev. Lett. **40** (1978) 38-41.
[21] RUNOV, A.M., *et al.*, Phys. Plasmas **8** (2001) 916.
[22] WATKINS, J.G., *et al.*, J. Nucl. Mater. In press (2006).
[23] ROEDER, R.K.W., RAPOPORT, B.I., and EVANS, T.E., Phys. Plasmas **10** (2003) 3796.
[24] FENSTERMACHER, M.E., *et al.,* J. Nucl. Mater. In press (2006).
[25] EVANS, T.E., *et al.,* J. Nucl Mater. In press (2006).